AIP | Applied Physics Letters

Magnetization reversal in Nd-Fe-B based nanocomposites as seen by magnetic small-angle neutron scattering

Jens-Peter Bick, Dirk Honecker, Frank Döbrich, Kiyonori Suzuki, Elliot P. Gilbert et al.

Citation: Appl. Phys. Lett. **102**, 022415 (2013); doi: 10.1063/1.4776708
View online: http://dx.doi.org/10.1063/1.4776708
View Table of Contents: http://apl.aip.org/resource/1/APPLAB/v102/i2
Published by the American Institute of Physics.

Magnetization reversal in Nd-Fe-B based nanocomposites as seen by magnetic small-angle neutron scattering

Jens-Peter Bick,[1] Dirk Honecker,[1] Frank Döbrich,[1] Kiyonori Suzuki,[2] Elliot P. Gilbert,[3] Henrich Frielinghaus,[4] Joachim Kohlbrecher,[5] Jorge Gavilano,[5] Edward M. Forgan,[6] Ralf Schweins,[7] Peter Lindner,[7] Rainer Birringer,[8] and Andreas Michels[1,a)]

[1]*Laboratory for the Physics of Advanced Materials, University of Luxembourg, 162A Avenue de la Faïencerie, L-1511 Luxembourg, Luxembourg*
[2]*Department of Materials Engineering, Monash University, Clayton, Victoria 3800, Australia*
[3]*Bragg Institute, Australian Nuclear Science and Technology Organisation, Locked Bag 2001, Kirrawee DC, NSW 2232, Australia*
[4]*Jülich Centre for Neutron Science, Lichtenbergstraße 1, D-85747 Garching, Germany*
[5]*Paul Scherrer Institut, CH-5232 Villigen PSI, Switzerland*
[6]*School of Physics and Astronomy, University of Birmingham, Birmingham B15 2TT, United Kingdom*
[7]*Institut Laue-Langevin, 6 Rue Jules Horowitz, B.P. 156, F-38042 Grenoble Cedex 9, France*
[8]*Experimentalphysik, Universität des Saarlandes, Postfach 151150, D-66041 Saarbrücken, Germany*

(Received 24 October 2012; accepted 3 January 2013; published online 16 January 2013)

We have studied the magnetization-reversal process of a $Nd_2Fe_{14}B/Fe_3B$ nanocomposite using small-angle neutron scattering. Based on the computation of the autocorrelation function of the spin misalignment, we have estimated the characteristic size l_C of spin inhomogeneities around the $Nd_2Fe_{14}B$ nanoparticles. The quantity l_C approaches a constant value of about 12.5 nm (∼average $Nd_2Fe_{14}B$ particle radius) at 14 T and takes on a maximum value of about 18.5 nm at the coercive field of −0.55 T. The field dependence of l_C can be described by a model that takes into account the convolution relationship between the nuclear and the magnetic microstructure. © *2013 American Institute of Physics*. [http://dx.doi.org/10.1063/1.4776708]

Rare-earth metals are key ingredients of countless technological products, and the global demand for these materials has continuously increased during the last decades. In recent times, geopolitical and strategic issues as well as the danger of a strained supply chain have caused the rare-earth elements to become the focus of attention of a wider public, and the term "critical raw materials" was coined for them.[1]

One of the most important fields of application of rare-earth metals are in high-performance permanent magnets, which are used, e.g., in electronics devices or motors. Nowadays, permanent magnets made out of the rare-earth transition-metal compounds Nd-Fe-B or Sm-Co possess a worldwide market share of about 65%.[2] Essentially, the rare-earth atoms in such alloys provide a high magnetic anisotropy, which results in broad hysteresis loops with intrinsic coercivities of the order of a few tesla, and the 3*d* transition-metal atoms give rise to a large magnetization along with a relatively high Curie temperature and a remanence of up to 1.5 T.[3–8]

Given that commercial-grade sintered Nd-Fe-B magnets are rare-earth rich[7] and in view of the above sketched situation, it is one of the central problems in the field of magnetic materials to search for strategies to reduce the amount of rare-earth elements by maintaining at the same time the magnets' performance.[2] Hard magnetic *nanocomposites*[9] are considered to be promising candidates for future permanent-magnet applications.[10] The microstructure of these materials consists of a dispersion of hard magnetic Nd-Fe-B or Sm-Co based nanoparticles that are embedded in and magnetically exchange-coupled to a soft magnetic transition-metal rich phase. As a consequence of the nanocomposites' reduced rare-earth content, production costs may be significantly lowered as compared to their sintered counterparts. Due to the technological relevance of such functional magnetic nanomaterials, a better understanding of the microstructure-property relationship is crucial, in particular, the magnetization-reversal process and the role of the thickness of the intergranular soft phase for magnetic hardening.[10–14]

In the present experiment, we have scrutinized the characteristic magnetic length scales associated with spin disorder during the magnetization-reversal process in a $Nd_2Fe_{14}B/Fe_3B$ nanocomposite. For this purpose, we have employed the technique of magnetic small-angle neutron scattering (SANS), which provides access to bulk properties on the interesting nanometer length scale.[15–28]

The SANS experiment was performed at the instrument Quokka at the Bragg Institute, ANSTO, Australia.[29] We used unpolarized incident neutrons with a mean wavelength of $\lambda = 5.1$ Å and with a bandwidth of $\Delta\lambda/\lambda = 10\,\%$ (FWHM). The external magnetic field was provided by a superconducting magnet which had the field direction perpendicular to the wave vector of the incoming neutron beam ($\mathbf{k}_0 \perp \mathbf{H} \parallel \mathbf{e}_z$) and in the plane of the ribbon sample (for sample details, see below). Using three sample-to-detector distances, this setup results in an accessible q-range of $0.03\,\mathrm{nm}^{-1} \lesssim q \lesssim 1.5\,\mathrm{nm}^{-1}$. SANS raw data were corrected for background scattering and detector efficiency. The autocorrelation function of the spin misalignment $C(r)$ was computed by means of the Fourier-transformation technique within the interval $r_{\min} = 2\pi/q_{\max} \cong 4$ nm and $r_{\max} = \pi/q_{\min} \cong 100$ nm. In order to reduce termination effects in the numerical calculation of $C(r)$, the

a)Author to whom correspondence should be addressed. Electronic mail: andreas.michels@uni.lu.

experimental SANS data beyond q_{max} were extrapolated to infinity using Porod's law, $d\Sigma_M/d\Omega \propto q^{-4}$, and the extrapolation from q_{min} to $q=0$ was carried out using different schemes (linear and constant).

The sample under study was a nanocrystalline hard magnetic composite, which was synthesized by the melt-spinning technique followed by rapid thermal annealing (10 min at 650 °C). The nominal composition of the amorphous precursor material was $Nd_5Fe_{74}Cr_3B_{18}$. As reported in Ref. 30, the microalloying of Cr supports the formation of the hard magnetic 2-14-1 phase and retards the formation of crystallization products with magnetically unfavorable properties. The two-phase microstructure of the nanocomposite consists of hard magnetic $Nd_2Fe_{14}B$ and soft magnetic Fe_3B crystallites.[30,31] Specimens that are prepared under such annealing conditions typically contain a $Nd_2Fe_{14}B$ particle volume fraction of about 45%.[30] Scanning and energy-filtered transmission electron microscopy was employed for the estimation of the respective average crystallite sizes: The average $Nd_2Fe_{14}B$ (Fe_3B) particle size is about 22 nm (29 nm). For the SANS experiments, several $Nd_2Fe_{14}B/Fe_3B$ ribbons (thickness: 20 μm; width: 2 mm; length: 10 mm) were stacked and arranged next to each other in order to completely cover the neutron aperture. Neutron absorption was reduced by employing low-capturing ^{11}B for the synthesis of the SANS sample.

For the above specified scattering geometry, the elastic nuclear and magnetic SANS cross section $d\Sigma/d\Omega$ at momentum-transfer vector $\mathbf{q}$ reads[32]

$$\frac{d\Sigma}{d\Omega}(\mathbf{q}) = \frac{8\pi^3}{V} b_H^2 (|\tilde{N}|^2/b_H^2 + |\tilde{M}_x|^2 + |\tilde{M}_y|^2 \cos^2\theta + |\tilde{M}_z|^2 \sin^2\theta - (\tilde{M}_y\tilde{M}_z^* + \tilde{M}_y^*\tilde{M}_z)\sin\theta\cos\theta), \quad (1)$$

where V is the scattering volume, $b_H = 2.9 \times 10^8 A^{-1}m^{-1}$, the superscript "*" refers to the complex-conjugated quantity, and $\tilde{N}(\mathbf{q})$ and $\tilde{M}(\mathbf{q}) = [\tilde{M}_x(\mathbf{q}), \tilde{M}_y(\mathbf{q}), \tilde{M}_z(\mathbf{q})]$ represent, respectively, the nuclear and magnetic scattering amplitudes. In the small-angle limit $\mathbf{q} \cong q\,(0, \sin\theta, \cos\theta)$, where the angle θ is measured relative to $\mathbf{e}_z$.

Figure 1 displays $d\Sigma/d\Omega$ of the $Nd_2Fe_{14}B/Fe_3B$ nanocomposite at 300 K and at selected applied magnetic fields H. The SANS experiments were performed by first applying a large positive field and then reducing the field to the experimental value, following the course of the hysteresis loop (see inset in Fig. 1). On decreasing the field starting from a value of $\mu_0 H = +10$ T (close to saturation), we observe the emergence of long-range magnetization fluctuations at the smallest momentum transfers. The total nuclear and magnetic $d\Sigma/d\Omega$ continues increasing up to a negative field value close to the experimental coercive field of $\mu_0 H_c = -0.55$ T. Further increase of H towards more negative values results in a suppression of magnetization fluctuations and in a concomitant decrease of $d\Sigma/d\Omega$ (open symbols in Fig. 1).

It is the central aim of this study to quantify the length scale and the applied-field dependence of spin-misalignment fluctuations during magnetization reversal in Nd-Fe-B based nanocomposites. From this point of view, and in order to

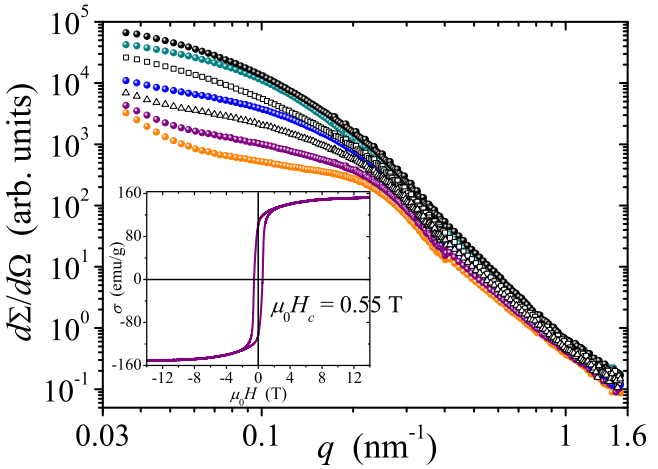

FIG. 1. Azimuthally-averaged total SANS cross section $d\Sigma/d\Omega$ of $Nd_2Fe_{14}B/Fe_3B$ as a function of momentum transfer q and applied magnetic field H ($T = 300$ K). Solid circles (●): H values (in Tesla) decrease from bottom to top: 10, 6, 1, −0.25, −0.55; (□): −1 T; (△): −3 T. Inset: Room-temperature magnetization curve of $Nd_2Fe_{14}B/Fe_3B$.

compute the associated correlation function of the spin misalignment, it would be advantageous to separate [in Eq. (1)] the spin-misalignment scattering from the scattering at complete magnetic saturation, where $d\Sigma/d\Omega = \frac{8\pi^3}{V}(|\tilde{N}|^2 + b_H^2 |\tilde{M}_z|^2 \sin^2\theta)$.

For a magnetic two-phase particle-matrix system close to saturation $|\tilde{M}_z|^2 \propto (\Delta M)^2$, where ΔM is the jump in the magnitude of the magnetization at the interface between the particles and the matrix. This jump is quite small for our nanocomposite, $\mu_0 \Delta M \cong 0.01$ T,[33] suggesting that the scattering due to $|\tilde{M}_z|^2$ correlations is much smaller than the nuclear SANS. Since $|\tilde{N}|^2$ is field-independent and in view of the strong field dependence of $d\Sigma/d\Omega$ (compare Fig. 1), it is obvious that the dominating contribution to $d\Sigma/d\Omega$ is due to transversal spin misalignment [compare Eq. (1)]. In order to obtain the associated spin-misalignment SANS cross section

$$\frac{d\Sigma_M}{d\Omega}(\mathbf{q}) = \frac{8\pi^3}{V} b_H^2 (|\tilde{M}_x|^2 + |\tilde{M}_y|^2 \cos^2\theta - (\tilde{M}_y\tilde{M}_z^* + \tilde{M}_y^*\tilde{M}_z)\sin\theta\cos\theta), \quad (2)$$

we assume in the following that the measured $d\Sigma/d\Omega$ at the highest field of 10 T represents to a good approximation the scattering at saturation (compare magnetization curve in Fig. 1). This assumption is supported (besides the $\sigma(H)$ data) by the finding that (1) the total $d\Sigma/d\Omega$ at 10 T exhibits an isotropic intensity distribution (data not shown), in other words, $d\Sigma/d\Omega$ at 10 T is essentially of nuclear origin; and (2) the total $d\Sigma/d\Omega$ at 10 T can (asymptotically) be described by a power-law $d\Sigma/d\Omega \propto q^{-4}$, as is characteristic for particle scattering (compare Fig. 2).[34] Subtraction of the (one-dimensional) 10 T data set from the $d\Sigma/d\Omega$ at the lower fields then yields $d\Sigma_M/d\Omega$.

The resulting data for $d\Sigma_M/d\Omega$ are shown in Fig. 3. Note also that as a consequence of the smallness of the $\tilde{M}_z$ scattering (relative to the transversal contributions), the cross term $\propto \tilde{M}_y\tilde{M}_z$ in $d\Sigma_M/d\Omega$ may be much smaller than the other terms. The magnitude of $d\Sigma_M/d\Omega$ is comparable to the

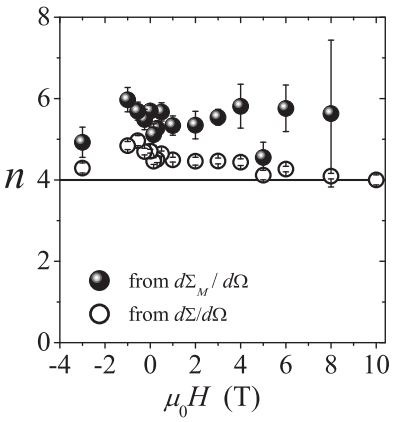

FIG. 2. Field dependence of the power-law exponent n which was determined by a fit of, respectively, $d\Sigma/d\Omega$ (Fig. 1) and $d\Sigma_M/d\Omega$ (Fig. 3) to K/q^n (K = constant). In both cases, the fit was restricted to the interval $0.6\,\mathrm{nm}^{-1} \le q \le 0.7\,\mathrm{nm}^{-1}$. Solid horizontal line: $n = 4$.

magnitude of the total $d\Sigma/d\Omega$ but, remarkably, $d\Sigma_M/d\Omega$ exhibits a significantly different shape than $d\Sigma/d\Omega$. In particular, the shoulder in $d\Sigma/d\Omega$ at $q \cong 0.2\,\mathrm{nm}^{-1}$ (compare Fig. 1) is absent in $d\Sigma_M/d\Omega$. Possible origins for the shoulder in $d\Sigma/d\Omega$ are interparticle interferences and/or diffusion zones around the particles.[15] Between +8 T (data not shown) and −0.55 T, $d\Sigma_M/d\Omega$ (at the smallest q) increases by a factor of about 180. The asymptotic power-law exponent n in $d\Sigma_M/d\Omega = K/q^n$ is at all fields investigated significantly larger than the value $n = 4$ (compare Fig. 2). These findings support the notion of dominant spin-misalignment SANS, which may give rise to power laws as steep as $d\Sigma_M/d\Omega \propto q^{-8}$ (Refs. 32 and 35).

The correlation function of the spin misalignment $C(r)$ was computed from the $d\Sigma_M/d\Omega$ data via[36,37]

$$C(r) = \frac{\alpha}{r}\int_0^\infty \frac{d\Sigma_M}{d\Omega}\sin(qr)\,q\,dq, \tag{3}$$

where α is a numerical constant; note that for the determination of the spin-misalignment length l_C the absolute value of α is not relevant. The field-dependent $C(r)$ calculated according to Eq. (3) are shown in Fig. 4(a) on a semi-logarithmic scale. In agreement with the previous discussion, it is clearly seen that the spin-misalignment correlations do not decay exponentially, which would yield (asymptotically) $d\Sigma_M/d\Omega \propto q^{-4}$ (compare Fig. 2). From the $C(r)$ data, we determined the spin-misalignment length $l_C(H)$ [see Fig. 4(b)]; l_C at a particular field was identified with the r value for which the correlation function has decayed to $\exp(-1)$ of its value at the origin $C(0)$, where the latter quantity was estimated by extrapolating $C(r)$ from $r_{\min}$ to $r = 0$ according to $C(r) \cong C(0) - ar^2$ [dotted line in Fig. 4(a)]. The neglect of a linear term in the above small-r expansion of $C(r)$ is consistent with the absence of a sharp interface in the magnetic microstructure (scattering from infinitely extended magnetization profiles).[34]

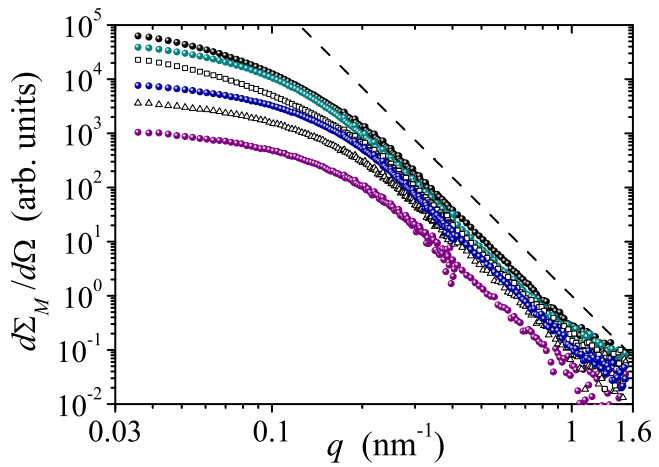

FIG. 3. Applied-field dependence of the spin-misalignment SANS cross section $d\Sigma_M/d\Omega$ of nanocrystalline $Nd_2Fe_{14}B/Fe_3B$ ($T = 300$ K). Solid circles (●): H values (in Tesla) decrease from bottom to top: 6, 1, −0.25, −0.55; (□): −1 T; (△): −3 T. Dashed line: $d\Sigma_M/d\Omega \propto q^{-5.5}$.

The length l_C is a measure of the size of gradients (around lattice imperfections) in the spin microstructure.[32,35,38] In the present case, it is expected that l_C describes the spatial extent of such magnetization inhomogeneities, mainly within the soft magnetic Fe_3B grains, that are caused by the jump in the magnetic materials parameters (exchange constant, magnetization, direction, and magnitude of magnetic anisotropy) at the interface between the $Nd_2Fe_{14}B$ particles and the surrounding Fe_3B crystallites [see inset in Fig. 4(b)].[39] The local perturbation of the magnetization at the phase boundary is transmitted by means of the exchange interaction into the soft phase.[38] As can be seen in Fig. 4(b), l_C approaches a constant value of about 12.5 nm at the largest positive fields and increases with decreasing applied field to take on a maximum value of about 18.5 nm at the experimental coercive field of $\mu_0 H_c = -0.55$ T. Further increase of H towards more negative values results again in a decrease of l_C towards ~12.5 nm.

The difference between the $l_C(H)$ data obtained at D11 (ILL) and at Quokka (ANSTO) is related to the fact that at D11 the incoming neutron wave vector was parallel to the applied magnetic field, whereas $\mathbf{k}_0 \perp \mathbf{H}$ at Quokka (and KWS 1). This entails a different SANS cross section and results in the slightly different values for l_C.[40] On top of that, one has to take into account the different demagnetizing-field effects for both geometries.

For such a scenario, it was shown that the following expression describes the field dependence of l_C,[32,35]

$$l_C(H_i) = \mathcal{L} + l_H(H_i), \tag{4}$$

where the field-independent parameter $\mathcal{L}$ is of the order of the particle size and $l_H = \sqrt{2A/(\mu_0 M_s H_i)}$ denotes the exchange length of the field with A the exchange constant and H_i the internal magnetic field. Note that $\mathcal{L} \cong R$ for spherical particles (of radius R) with a uniform magnetic anisotropy field.[35] Equation (4) embodies the convolution relationship between the magnetic anisotropy field microstructure ($\mathcal{L}$) and the magnetic microstructure (l_H).

However, due to irregularities in the shape of the ribbon sample and due to nonzero volume divergences of the magnetization, the precise value of the internal field H_i in Eq. (4) is not known. Since in the SANS experiments the applied field H is the control parameter, we set $H_i = H + H^\star$ in Eq. (4) in order to compare the experimental $l_C(H)$ data with the

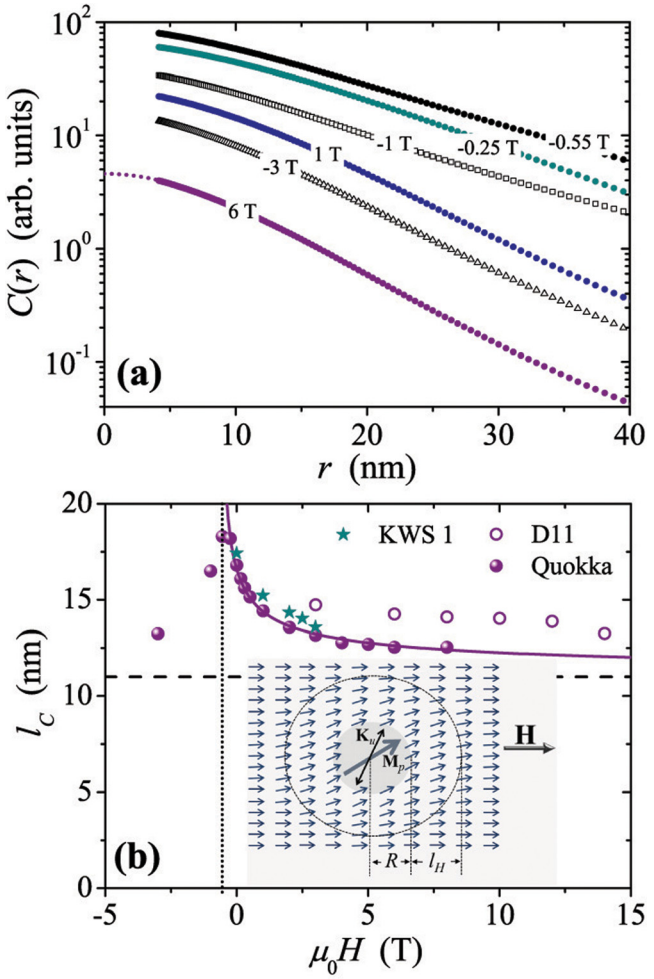

FIG. 4. (a) Field dependence of the correlation function $C(r)$ of the spin misalignment of nanocrystalline $Nd_2Fe_{14}B/Fe_3B$ (semi-logarithmic scale). The field values follow the course of a hysteresis loop, starting from a large positive field and then reducing the field to negative values. Dotted line (extrapolating the 6 T data to $r=0$): $C(r)=4.58-0.043\,r^2$. (b) Field dependence of the spin-misalignment length l_C. Solid line: fit of the data to $l_C(H)=\mathcal{L}+\sqrt{2A/[\mu_0 M_s(H+H^\star)]}$, where $\mathcal{L}=10.9$ nm and $\mu_0 H^\star=+0.60$ T are treated as adjustable parameters; the quantities $A=12.5$ pJ/m and $\mu_0 M_s=1.6$ T are held fixed. For comparison, $l_C(H)$ data obtained at the SANS instruments KWS 1 (JCNS, Germany) and D11 (ILL, France) are included. Dashed horizontal line: average $Nd_2Fe_{14}B$ particle radius $R=11$ nm. Dotted vertical line: experimental coercive field $\mu_0 H_c=-0.55$ T. Inset: Sketch illustrating the meaning of $l_C=R+l_H$. In the presence of an applied magnetic field $\mathbf{H}$, the magnetization $\mathbf{M}_p$ of the $Nd_2Fe_{14}B$ particle may be tilted away from the strong uniaxial anisotropy axis $\mathbf{K}_u$ of the particle. The jump in the materials parameters at the "hard-soft" interface (here, predominantly $\mathbf{K}_u$ fluctuations) gives rise to spin disorder that is transmitted via the exchange interaction (on a decay length l_H) into the soft magnetic Fe_3B crystallites.

theoretical prediction; $H^\star$ is expected to model the influence of the magnetodipolar field and of the magnetic anisotropy.[41] The solid line in Fig. 4(b) is the result of a fit of the, in this way, modified Eq. (4) to the $l_C(H)$ data. We obtain $\mathcal{L}=10.9$ nm (close to the experimental average grain radius of the $Nd_2Fe_{14}B$ phase) and $\mu_0 H^\star=+0.60$ T, which is close to the absolute value of the experimental coercive field.

It has been predicted[10–14] that an optimum magnetic hardness of two-phase hard/soft nanocomposites is obtained, if the size of the magnetically soft phase is smaller than about twice the domain-wall width $\delta_B=\pi\sqrt{A/K_1}$ of the hard magnetic phase ($\delta_B\cong 4.2$ nm for $Nd_2Fe_{14}B$). By means of the presented methodology it becomes possible to address this question in more detail in the future, in particular, one can relate macroscopic magnetic properties and the size of the soft-phase grains (here: ~15 nm) to an estimate for the size of inhomogeneously magnetized regions: In the remanent state, we find $l_C\cong 17$ nm which (after subtraction of $\mathcal{L}$) suggests a penetration depth of the spin disorder into the soft magnetic phase of about 5–6 nm. The sketched picture presupposes that the $Nd_2Fe_{14}B$ crystallites are essentially in a single-domain state [compare also inset in Fig. 4(b)].

In summary, we have presented an analysis of magnetic SANS data in terms of the autocorrelation function of the spin misalignment, which allows one to study the magnetization-reversal process of magnetic materials. For a $Nd_2Fe_{14}B/Fe_3B$ nanocomposite, we have estimated the characteristic size of spin inhomogeneities around the $Nd_2Fe_{14}B$ nanoparticles. Our results for the spin-misalignment length l_C reveal an increase of l_C with decreasing applied field with a maximum of about 18.5 nm at the experimental coercive field of $\mu_0 H_c=-0.55$ T. In the remanent state, the size of gradients in the magnetization within the soft magnetic Fe_3B phase is estimated to about 5–6 nm. A modified version of Eq. (4) provides an excellent description of the field dependence of the spin-misalignment correlations.

We thank the DFG (Project No. MI 738/6-1) and the FNR of Luxembourg (ATTRACT Project No. FNR/A09/01 and AFR Project No. 896446) for financial support.

[1]P. C. Dent, J. Appl. Phys. **111**, 07A721 (2012).
[2]O. Gutfleisch, M. A. Willard, E. Brück, C. H. Chen, S. G. Sankar, and J. P. Liu, Adv. Mater. **23**, 821 (2011).
[3]J. J. Croat, J. F. Herbst, R. W. Lee, and F. E. Pinkerton, J. Appl. Phys. **55**, 2078 (1984).
[4]M. Sagawa, S. Fujimura, N. Togawa, H. Yamamoto, and Y. Matsuura, J. Appl. Phys. **55**, 2083 (1984).
[5]K. H. J. Buschow, Rep. Prog. Phys. **54**, 1123 (1991).
[6]G. C. Hadjipanayis, J. Magn. Magn. Mater. **200**, 373 (1999).
[7]O. Gutfleisch, A. Bollero, A. Handstein, D. Hinz, A. Kirchner, A. Yan, K.-H. Müller, and L. Schultz, J. Magn. Magn. Mater. **242–245**, 1277 (2002).
[8]J. Fidler, T. Schrefl, S. Hoefinger, and M. Hajduga, J. Phys.: Condens. Matter **16**, S455 (2004).
[9]R. Coehoorn, D. B. de Mooij, and C. de Waard, J. Magn. Magn. Mater. **80**, 101 (1989).
[10]J. P. Liu, in *Nanoscale Magnetic Materials and Applications*, edited by J. P. Liu, E. Fullerton, O. Gutfleisch, and D. J. Sellmyer (Springer, New York, 2009), pp. 309–335.
[11]E. F. Kneller and R. Hawig, IEEE Trans. Magn. **27**, 3588 (1991).
[12]T. Schrefl, H. Kronmüller, and J. Fidler, J. Magn. Magn. Mater. **127**, L273 (1993).
[13]R. Skomski and J. M. D. Coey, Phys. Rev. B **48**, 15812 (1993).
[14]R. Fischer, T. Leineweber, and H. Kronmüller, Phys. Rev. B **57**, 10723 (1998).
[15]A. Heinemann, H. Hermann, A. Wiedenmann, N. Mattern, and K. Wetzig, J. Appl. Crystallogr. **33**, 1386 (2000).
[16]A. Michels, J. Weissmüller, A. Wiedenmann, and J. G. Barker, J. Appl. Phys. **87**, 5953 (2000).
[17]A. Michels, J. Weissmüller, A. Wiedenmann, J. S. Pedersen, and J. G. Barker, Philos. Mag. Lett. **80**, 785 (2000).
[18]A. Michels, R. N. Viswanath, and J. Weissmüller, Europhys. Lett. **64**, 43 (2003).
[19]W. Wagner and J. Kohlbrecher, in *Modern Techniques for Characterizing Magnetic Materials*, edited by Y. Zhu (Kluwer Academic, Boston, 2005), pp. 65–103.
[20]J. F. Löffler, H. B. Braun, W. Wagner, G. Kostorz, and A. Wiedenmann, Phys. Rev. B **71**, 134410 (2005).

[21]T. Thomson, S. L. Lee, M. F. Toney, C. D. Dewhurst, F. Y. Ogrin, C. J. Oates, and S. Sun, Phys. Rev. B **72**, 064441 (2005).
[22]B. van den Brandt, H. Glättli, I. Grillo, P. Hautle, H. Jouve, J. Kohlbrecher, J. A. Konter, E. Leymarie, S. Mango, R. P. May, A. Michels, H. B. Stuhrmann, and O. Zimmer, Eur. Phys. J. B **49**, 157 (2006).
[23]A. Michels, C. Vecchini, O. Moze, K. Suzuki, P. K. Pranzas, J. Kohlbrecher, and J. Weissmüller, Phys. Rev. B **74**, 134407 (2006).
[24]A. Michels, F. Döbrich, M. Elmas, A. Ferdinand, J. Markmann, M. Sharp, H. Eckerlebe, J. Kohlbrecher, and R. Birringer, EPL **81**, 66003 (2008).
[25]S. J. Lister, T. Thomson, J. Kohlbrecher, K. Takano, V. Venkataramana, S. J. Ray, M. P. Wismayer, M. A. de Vries, H. Do, Y. Ikeda, and S. L. Lee, Appl. Phys. Lett. **97**, 112503 (2010).
[26]K. L. Krycka, R. A. Booth, C. R. Hogg, Y. Ijiri, J. A. Borchers, W. C. Chen, S. M. Watson, M. Laver, T. R. Gentile, L. R. Dedon, S. Harris, J. J. Rhyne, and S. A. Majetich, Phys. Rev. Lett. **104**, 207203 (2010).
[27]C. Dufour, M. R. Fitzsimmons, J. A. Borchers, M. Laver, K. L. Krycka, K. Dumesnil, S. M. Watson, W. C. Chen, J. Won, and S. Singh, Phys. Rev. B **84**, 064420 (2011).
[28]S. Disch, E. Wetterskog, R. P. Hermann, A. Wiedenmann, U. Vainio, G. Salazar-Alvarez, L. Bergström, and T. Brückel, New J. Phys. **14**, 013025 (2012).
[29]E. P. Gilbert, J. C. Schulz, and T. J. Noakes, Physica B: Condensed Matter **385–386**, 1180 (2006).
[30]K. Suzuki, J. M. Cadogan, M. Uehara, S. Hirosawa, and H. Kanekiyo, Scr. Mater. **42**, 487 (2000).
[31]J. C. Shih, A. J. Saldanha, K. Suzuki, T. Shoji, A. Kato, and S. Tajima, J. Appl. Phys. **99**, 08B505 (2006).
[32]A. Michels and J. Weissmüller, Rep. Prog. Phys. **71**, 066501 (2008).
[33]T. Schrefl and J. Fidler, J. Magn. Magn. Mater. **177–181**, 970 (1998).
[34]G. Porod, in *Small Angle X-ray Scattering*, edited by O. Glatter and O. Kratky (Academic, London, 1982), pp. 17–51.
[35]A. Michels, Phys. Rev. B **82**, 024433 (2010).
[36]A. Michels, R. N. Viswanath, J. G. Barker, R. Birringer, and J. Weissmüller, Phys. Rev. Lett. **91**, 267204 (2003).
[37]J. Weissmüller, A. Michels, D. Michels, A. Wiedenmann, C. E. Krill III, H. M. Sauer, and R. Birringer, Phys. Rev. B **69**, 054402 (2004).
[38]H. Kronmüller and A. Seeger, J. Phys. Chem. Solids **18**, 93 (1961).
[39]R. Skomski, J. Phys.: Condens. Matter **15**, R841 (2003).
[40]F. Döbrich, M. Elmas, A. Ferdinand, J. Markmann, M. Sharp, H. Eckerlebe, J. Kohlbrecher, R. Birringer, and A. Michels, J. Phys.: Condens. Matter **21**, 156003 (2009).
[41]W. F. Brown, Jr., IEEE Trans. Magn. **MAG-6**, 121 (1970).